Journal of Drug Delivery Science and Technology 89 (2023) 105080

Contents lists available at ScienceDirect

Journal of Drug Delivery Science and Technology

journal homepage: www.elsevier.com/locate/jddst

Synthesis of microsponges by spray drying TEMPO-oxidized cellulose nanofibers and characterization for controlled release

Andrea Fiorati [a], Francesca Baldassarre [b,c,*], Laura Riva [a], Stefano Tacconi [d], Concetta Nobile [c], Viviana Vergaro [b,c], Roberto Grisorio [e], Lucio Melone [a,f], Andrea Mele [a], Luciana Dini [d], Carlo Punta [a], Giuseppe Ciccarella [b,c]

[a] Department of Chemistry, Materials, and Chemical Engineering "G. Natta" and Local Unit INSTM, Politecnico di Milano Piazza Leonardo da Vinci 32, 20133, Milano, Italy
[b] Department of Biological and Environmental Sciences, UdR INSTM of Lecce University of Salento, Via Monteroni, 73100, Lecce, Italy
[c] Institute of Nanotechnology, CNR NANOTEC, Consiglio Nazionale delle Ricerche, Via Monteroni, 73100, Lecce, Italy
[d] Department of Biology and Biotechnology "Charles Darwin", University of Rome "La Sapienza", Piazzale Aldo Moro 5, 00185, Roma, Italy
[e] Department of Civil, Environmental, Land, Construction Engineering and of Chemistry (DICATECh), Polytechnic University of Bari, Via Orabona 4, Bari, 70125, Italy
[f] Centro di Ricerca per l'Energia, l'Ambiente e il Territorio (CREAT), Università Telematica eCampus, Novedrate, CO, 22060, Italy

ARTICLE INFO

Keywords:
TEMPO oxidized cellulose nanofibers
Spray drying
Crosslinking
Microsponges
Controlled drug release

ABSTRACT

A Spray Drying process is presented for one-step production of nanostructured microsponges from TEMPO oxidized cellulose nanofibers (TOCNF). Different formulations were prepared by varying both the nanofibers oxidation degree and the relative ratios of branched polyethyleneimine and citric acid, introduced as cross-linkers. The best reaction conditions were achieved using TOCNF containing the highest content of carboxylic groups (1.5 $mmol_{COOH}/g_{TOCNF}$), which produced microparticles with an average diameter below 5 μm, and a good colloidal stability in aqueous dispersion. Physical-chemical characterization was carried out to study the chemical bonds in the microsponges matrix, the swelling degree and drug loading and release. Tetracycline, a broad-spectrum drug with pH-dependent amphoteric feature, was chosen as model molecule. Chemical cross-linking was verified by spectroscopic characterisation, which revealed the formation of amide bonds. The crosslinked microsponges showed a high drug loading efficiency, as opposed to non-cross-linked ones, and a pH-responsivity in terms of swelling and drug release behaviour. Finally, microsponges derived from formulations without citric acid resulted biocompatible, as demonstrated by direct and indirect *in vitro* tests on gastric cancer cells.

1. Introduction

The interest in the entrapment of bioactive molecules and therapeutic compounds in polymeric scaffolds for targeted applications is continuously growing. In this scenario, microparticles (MP), microsponges (MS) by which nanoparticles with tuneable properties and obtained from biodegradable/biocompatible polymers stand out as state-of-the-art systems [1–4]. The preparation of polymeric systems involves various strategies including the use of metal salts and crosslinking agents, hydrothermal/solvothermal synthesis, evaporation of emulsions and solvents, precipitation methods with or without crosslinking agents and supercritical precipitation in anti-solvents [5,6]. Nanocellulose, either in the form of cellulose nanofibers (CNF) or cellulose nanocrystals (CNC), can be processed or chemically modified in various ways to produce drug delivery carriers, microreactors and scaffolds for tissue engineering [5,7,8]. In particular, CNF have been reported as versatile building blocks for the preparation of carriers with different morphologies, including particles, capsules, films, aerogels, wet-stable foams and hydrogels [9–12]. The interest in CNF as drug delivery platform is related to their unique physical-chemical properties, biocompatibility, and large surface area-to-volume ratio. Cellulose chemistry promotes molecular interactions with poorly soluble drugs, stabilization of drugs nanocrystals and smart chemical modifications [11]. In recent years, the oxidation of CNF with (2,2,6,6-tetramethylpiperidine-1-oxyl) stable radical (TEMPO) has emerged as a simple, efficient, versatile, mild and inexpensive synthetic route to a new type of fibers, referred to as

* Corresponding author. Department of Biological and Environmental Sciences, UdR INSTM of Lecce University of Salento, Via Monteroni, 73100 Lecce, Italy.
E-mail address: francesca.baldassarre@unisalento.it (F. Baldassarre).

https://doi.org/10.1016/j.jddst.2023.105080
Received 7 June 2023; Received in revised form 26 September 2023; Accepted 16 October 2023
Available online 21 October 2023

TEMPO-oxidized cellulose nanofibers (TOCNF) [13] These nanofibers have been widely investigated by Isogai et al. in terms of both thermal and pH stability [14]. They found that no depolymerization occurred on TOCNF in water at pH 1.0–7.0 and room temperature, while partial depolymerization by β-elimination could occur at temperatures higher than 50 °C and at pH > 10. TOCNF were used directly as additives for the production of composites, and to fabricate aerogels with low density and high surface area [15,16] for a range of applications, such as water remediation, drug delivery and tissue engineering [7]. Moreover, TOCNF can be easily chemically modified to introduce desired properties [11,17].

In this context, it is worth noting that, the synthesis of nanocellulose-based carriers could be achieved by the Spray Drying Technology (SDT). However, the literature reports few examples of preparations from aqueous suspensions of mainly bacterial cellulose nanofibers, mechanically treated CNF, and CNC [18–21]. This finding is unexpected considering that SDT is a dehydration process widely used in food, pharmaceutical, and chemical industries [22]. STD is a one-step particles synthesis method based on the fast evaporation of the solvent, atomized in a plume of liquid droplets, resulting in the formation of a multi-particle dry powder containing the product of interest [23,24]. The STD process is simple, easily scalable, generally less expensive than other techniques such as supercritical fluid drying and freeze drying, and with mild thermal effects due to the short contact time of the atomized droplets with the hot drying media [25]. Powders obtained via SDT have better dispersibility than those from other competing techniques [26]. This feature is important for CNF processing, as they are usually synthesized and modified in aqueous environment, and thus require an efficient drying step. Furthermore, STD allows to tune operating parameters controlling size and morphology of the dried CNF particles [27].

In the last years, we reported a new class of sponge-like materials obtained by crosslinking TOCNF with branched polyethylenimine (bPEI) and citric acid (CA). bPEI bears a high number of amine groups [28], with an amine density significantly higher if compared with most of the commercial cellulose-fiber coupling agents [29,30]. For this reason, it was chosen as an ideal crosslinker to promote the formation of amide bonds by reacting with the carboxylic groups of TOCNF. CA was further introduced in the formulation as additional source of carboxylic acid moieties, to increase the crosslinking degree and consequently, the chemical and mechanical stability of final materials [31]. The highly porous materials were obtained by mixing the three components in a water solution, freeze-drying the resulting gel-like dispersions, and finally undergoing the resulting aerogels to thermal treatment [31,32]. The materials so obtained showed good properties for drug delivery, anion sensing, heterogeneous catalysis, and water decontamination [33–35].

Herein we report on the use of SDT on TOCNF and bPEI aqueous formulations, in presence or not of CA as additional crosslinker, to produce tuneable nanostructured MS for drug delivery. Tetracycline (TC) was selected as model drug due its interesting physical-chemical and biological properties. TC is a broad-spectrum antibiotic, and it is also applied in dermatology for its many anti-inflammatory effects [36,37]. It is known as an antimetastatic drug, inhibiting the matrix metalloproteinases which trigger metastatic mechanisms in several malignant cancers [38]. Due to its intrinsic light sensitivity, TC requires carrier utilization for successful delivery and bioactivity. In addition, TC oral administration is affected by food intake due to the formation of TC-metal complexes that preclude gastrointestinal absorption. Furthermore, TC is a pH dependent amphoteric molecule due to the presence of three functional groups: the dimethylammonium group, the phenolic diketone moiety and the tricarbonyl methane group. TC exists predominantly as cation at pH < 3.3, as zwitterion at pH between 3.3 and 7.7, and as anion at pH > 7.7 [36]. So, it can be considered a good molecule model for drug release studies. TC loading in aqueous TOCNF-based MS suspensions was studied. The influence of the initial TOCNF formulations on SDT process parameters and on the derived MS properties was investigated and hereafter discussed. MS were characterized by FT-IR and ^{13}C CP-MAS NMR spectroscopies, SEM/STEM electron microscopy, TGA and DLS analysis. Physical-chemical properties, in terms of swelling degree, TC loading efficiency, and TC release kinetics were studied at different pH. Moreover, the *in vitro* cytocompatibility of the synthetized MS was assessed by indirect and direct contact tests towards human gastric carcinoma cells. The gathered data indicate that a thorough investigation of the Spray Drying process parameters and the introduction of chemical crosslinkers is necessary for the development of TOCNF-based microsponges as effective drug delivery systems.

Table 1
TOCNF-based stock formulations.

Entry	Sample	TOCNF (g)	bPEI (g)	Anhydrous citric acid (mg)	Water (mL)
1	**TOCNF**	3.5	0	0	350
2	**bPEI-TOCNF**	3.5	3.5	0	350
3	**bPEI-TOCNF@CA70**	3.5	3.5	70	350
4	**bPEI-TOCNF@CA140**	3.5	3.5	140	350

2. Materials and methods

2.1. Cellulose oxidation and TOCNF production

All the reagents were purchased from Sigma-Aldrich. Cotton linters cellulose was provided by Bartoli Spa paper mill (Capannori, Lucca, Italy). Deionized water was produced with a Millipore Elix® Deionizer with Progard® S2 ion exchange resins. Ultra-sonication process was carried out with a Branson Sonifier 250 equipped with a 6.5 mm probe tip. Cellulose with different oxidation degrees (0.5, 1, 1.3, 1.5 $mmol_{COOH}/g_{TOCNF}$) was prepared according to a procedure previously reported in the literature [13,39]. The procedures for oxidation and nanofiber production are detailed in the Supplementary Information. The list of the produced samples is in Table S1.

Spray dry parameters set-up: Each TOCNF sample of Table S1 was dispersed in water at three different concentrations (0.5, 1.0 and 2.0 w/v) and ultra-sonicated with a Branson SFX250 Sonicator (15 min constant-pulse, three cycles). During the dispersion process, the samples were kept in an ice bath and the pH was adjusted to 10 by dropwise addition of a solution of aqueous ammonia (25 % w/v).

The MS were synthesized using TOCNF with an oxidation degree of 1.5 $mmol_{COOH}/g_{TOCNF}$ (i.e. mmol of C6 alcoholic groups of glucopyranose units converted to the corresponding carboxylic moieties per gram of TOCNF). In order to prepare each of the 4 samples (see Table 1), 3.5 g of dried TOCNF were dispersed in 350 mL of deionized water. Stoichiometric NaOH pellets (5.25 mmol, 0.21 g) were added to the suspension and the mixture was ultra-sonicated with the aid of a Branson SFX250 Sonicator, keeping the temperature stable with an ice bath. Three cycles of constant-pulse ultrasonication of 15 min each are performed. After the last sonication cycle, 15 mL of HCl 0.5 N were added to the suspension and the mixture was then filtered over Büchner funnel and washed with deionized water until neutral pH, to remove the in situ formed NaCl. The resulting 4 wet solid samples were dispersed with deionized water until a final volume of 350 mL each (content of TOCNF: ≈1% w/v). When expected, bPEI and CA were dissolved into dispersions in the ratios as reported in Table 1 (entries 2–4). The mixtures were finally ultra-sonicated for 15 min in an ice bath.

2.2. Spray drying synthesis of TOCNF microsponges

The process was done on a Büchi Mini Spray Dryer B-290. TOCNF aqueous suspensions (concentrations 0.1, 0.5 and 1% w/v) were drawn

by a peristaltic pump with a flow rate of 4 mL/min and 2 mL/min. The solution was allowed to flow into a water-cooled two-fluid nozzle (nozzle diameter 1.4 mm) and sprayed at these process parameters: inlet temperature 210 and 220 °C, aspirator 100%, spray gas flow length 40 mm. Soon after the beginning of the spraying, a dry powder was formed. The powder was recovered at the collecting vessel and washed three times with water through centrifugations (3000 rpm for 10min). This washing step was achieved to eliminate potential chemicals residues. The samples were freeze-dried for storage before subsequent analyses. Dried samples were collected, weighed, and directly suspended in the target solvent for the specific analysis. The presence of free bPEI in the MS supernatants prior to characterization was excluded by a colorimetric test with complexation of copper cations adding aqueous solution of copper acetate (0.1 M).

2.3. Physicochemical and morphological characterization

2.3.1. Morphological analysis

Morphological characterization of TOCNF and TOCNF-based MS was done by transmission electron microscopy (TEM) and scanning/scanning-transmission electron microscopy (SEM/STEM). One drop of sample solution (10 μl) was placed on a standard TEM carbon-coated Cu grid and dried at room temperature. The grids were viewed under a JEOL JEM 1400Plus microscope at an accelerating voltage of 80 kV, for TEM acquisitions, and under a FESEM MERLIN ZEISS operating at an accelerating voltage of 20 kV, for SEM and ADF – STEM imaging. This setup allowed the simultaneous image collection in SEM and ADF – STEM mode of selected sample regions.

2.3.2. Chemical analysis

The solid samples were analysed by attenuated total reflectance (ATR) FT-IR on a Varian 640-IR spectrometer equipped with a single bounce ZnSe crystal. 64 acquisitions for each sample were collected. The ^{13}C cross-polarization magic-angle-spinning (^{13}C CP-MAS) NMR spectra were acquired on an Avance Neo 500 (Bruker BioSpin S.r.l) at 11.7 T corresponding to ^{13}C operating frequency of 125.76 MHz. The following conditions were applied: repetition time 4 s, ^{1}H 90 pulse length 4.0 ms, contact time 1.2 ms, and spin rate 8 kHz. The compounds were placed in a 4 mm zirconia rotor. The chemical shifts were referenced to glycine (C═O signal: 176.03 ppm). Powder XRD patterns were recorded on a Bruker D2 Phaser X-ray powder diffractometer using CuKα radiation. The data were collected in the 2θ range 7°–40° with a step size of 0.02° and a counting time of 0.4 s per step, a primary slit module of 0.6 mm, air scatter screen module 1 mm and secondary slit module of 8 mm.

2.3.3. Dynamic light scattering analysis

TOCNF and the MS were analysed with a Nano ZS90 (Malvern Instruments, UK) instrument for ζ-potential measure. The potential analysis of particles was carried out by Laser Doppler Velocimetry (LDV), with an appropriate sample dilution in distilled water. Samples dilution is necessary to obtain reliable measurements. Too concentrated samples lead to measurements affected by multiple scattering, thus providing inaccurate results and poor distribution data (by the quality report of Zetasizer Measurement software). Preliminary DLS tests indicated the optimum sample concentration of 0.01 mg/mL. The ζ-potential values are reported as the mean of 5 measurements; each of them derived from 10 different runs to establish measurement repeatability.

2.3.4. Swelling study

TOCNF MS swelling behaviour was examined through the gravimetric method. A known quantity of MS was soaked into buffer solutions (pH 2, 5, 7.5 and 11) and simulated gastric fluid (SGF) for 48h at room temperature. The SGF at pH 1.2 was prepared by adding 7 mL of concentrated HCl (37%) to 500 mL of distilled water. The solution was then added of 2 g of NaCl and more distilled water to a final volume of 1L [40].

The excess water on the swollen MS was removed by filter paper and the particles weighed. Taking the average value of three measurements for each sample, the swelling ratio percentage (SR) is calculated with equation (1):

$$\%\ SR = \frac{Ws - Wd}{Wd}\ x\ 100 \quad (1)$$

W_s and W_d are the weight of the swollen and dried MS, respectively.

2.3.5. Thermal analysis

Thermogravimetric analysis (TGA) was carried out on a TA Instruments Q600 instrument with 100 mL/min nitrogen flow and a 10 °C/min heating rate, as previously reported [41].

2.4. Drug loading study

The loading of TC (monohydrate form from Sigma Aldrich) within cellulose MS was carried out by adding, drop by drop, a drug mother solution (2.5 mg/mL in ethanol) to an aqueous dispersion of microsponges (100 mg) reaching the selected final concentration of 0.5 mg/mL. The physical adsorption was achieved by mixing overnight the suspension at RT, in the dark. The samples were then washed three times with water through centrifugations (3000 rpm for 10min).

The drug loading efficiency onto MS was evaluated by the UV–vis quantification of the free drug in the reaction supernatants to quantify indirectly the amount of drug loaded. The UV–Vis absorption spectra were recorded at 355 nm by a Varian-Cary 500 UV–Vis spectrophotometer. The unknown concentration was calculated with a standard curve obtained by using aqueous solutions of TC at a known concentration (0.5-0.25-0.12-0.06-0.03-0.01 mg/mL). The fitting line was obtained through Origin software by reporting the absorption values multiplied by the dilution factor *vs* concentrations (see Figure SI1 A).

Loading efficiency was calculated with equation (2):

$$\%\ loading\ efficiency = \frac{[loading\ solution] - [supernatant]}{[loading\ solution]}\ x\ 100 \quad (2)$$

where [loading solution] is the initial concentration of TC and [supernatant] is the drug concentration in the reaction supernatant (free TC).

The possible drug loss was assessed by the analysis of the washing supernatants. The loaded quantity is determined by subtraction, and it is used to calculate the loading capacity (equation (3)).

$$\%\ loading\ capacity = \frac{mg_{drug}}{mg_{microsponges}} * 100 \quad (3)$$

Where mg_{drug} is the estimated quantity of TC (by % loading efficiency data) onto MS after the loading procedure, $mg_{microsponges}$ is the exposed quantity of MS (100 mg).

The literature reports a wide use of the equations mentioned above to determine the loading procedures efficiency and the loading capacity of carriers in the case of different drugs, systems, and encapsulation methods [42–44].

2.5. In vitro drug release study

In vitro drug release profiles of the TOCNF MS were obtained by immersing a known quantity of TC-loaded samples (5 mg) into 1 mL of buffer solutions (pH 2, 5, 7.5 and 11) and SGF (pH 1.2) for increasing time intervals (1, 4, 6, 8, 24 and 48h).

The samples were incubated at room temperature and a constant agitation of 900 rpm. After a predetermined period, MS were precipitated through centrifugation (3.000 rpm for 10 min) and the released drug was quantified by the standard TC calibration curve. In Figure SI1 we report the used fitting lines with Absorption value multiplied by dilution factor *vs* concentration. The calibration curve at pH 2 in SI1C was used for the other acid condition (pH5 and SGF) because the TC

absorption did not change. All release studies were performed in triplicate. The results were presented in terms of cumulative percentage release as a function of time using equation (4):

$$Cumulative\ percentage\ release = \frac{W_t}{W_i}\ x\ 100 \quad (4)$$

where W_t is the amount of TC released from MS at time t and W_i is the amount of TC loaded onto the MS.

Dried samples were obtained by freeze-drying and W_i derived from % loading capacity data (eq. (3)). W_t derived from release supernatants quantification by UV–vis, considering the used volume of 1 mL.

2.6. Biocompatibility study

2.6.1. Cell culture and treatments

Human gastric carcinoma cells, Kato III (ATCC), were cultured in Roswell Park Memorial Institute (RPMI) 1640 medium (Cambrex, Verviers, BE) supplemented with 10% fetal bovine serum (Cambrex, Verviers, BE), 2 mM L-glutamine (Cambrex, Verviers, BE), 100 IU/mL penicillin and streptomycin solution and 10.000 U/mL amphotericin (antimycotic solution) (Sigma-Aldrich, St. Louis, MO) at 37 °C in 5% CO_2. Cells were maintained in 75 cm^2 flasks (concentration ranged between 2×10^5 and 1×10^6 cells/mL) by passage every 3–4 days when the culture reached approximately 80% confluence.

The viability study of Kato III cells was carried out by using both direct and indirect contact methods. About 10^4 cells seeded in 96-well plates were allowed to attach overnight before treatments. In the direct contact experiments, cells were incubated for 12 or 24 h with two TOCNF MS samples of concentration of 0.01 and 0.025 mg/mL, respectively. For the indirect contact experiments, TOCNF MS samples were first incubated in a complete culture medium for 24 h at 37 °C at concentrations of 0.1 mg/mL and 0.25 mg/mL. The conditioned culture medium was centrifuged at 3000 rpm for 30 min to remove the microparticles and then added to Kato III cells for 24 h. Incubation of cells with complete RPMI culture medium alone were used as control. TOCNF MS powder was sterilized through UV exposition for 2 h.

2.6.2. MTT assay

Cyto-viability was evaluated by 3-(4,5-dimethylthiazol-2-yl)-2,5-diphenyl tetrazolium bromide (MTT) assay. After each treatment, Kato III cells were incubated with 1 mg/mL of MTT, prepared in complete RPMI culture medium, for 3 h at 37 °C and 5% CO_2. The cells were then washed three times with phosphate buffer saline (PBS 0.2 M, pH 7,4) and the reduced MTT formazan crystals were solubilized with dimethyl sulfoxide (Carlo Erba, Milan, Italy). The optical density (OD) at 570 nm was measured with a MultiskanTM FC Microplate Photometer (ThermoFisher Scientific, Waltham, MA). Viability was expressed as a percentage of cells viability by equation (5):

$$\%\ Cells\ viability = \frac{A_{sample}}{A_{control}}\ x\ 100 \quad (5)$$

where A_{sample} and $A_{control}$ are the absorbance values of treated and non-treated cells, respectively. Data are reported as mean ± Standard Deviation of three independent experiments, each done in duplicate. Statistical significance was determined by Student t-test.

3. Results and discussion

3.1. TOCNF microsponges spray drying synthesis

The MS production from TOCNF and bPEI-TOCNF-based formulations and the physical-chemical properties of resulting particles were optimized by assessing the role of fibers oxidation degree, crosslinking degree and SDT process parameters. First, the TOCNF suspensions reported in Table S1 with different content of carboxylic groups, expressed as $mmol_{COOH}/g_{TOCNF}$, were tested at three concentrations (0.1, 0.5 and 1 % W/V). The TOCNF dispersions at oxidation degrees 0.5, 1.0, and 1.3 $mmol_{COOH}/g_{TOCNF}$ afforded small amounts of dry powder and gave pump lock after a few minutes, possibly for the formation of aggregates even at low concentrations (eye inspection). These suspensions could be used only at concentrations lower than 0.1% w/v, and were thus unsuitable for SDT. SDT is sensitive to drug and/or polymer solubility and concentration [8,45,46]. For this reason, CNF water dispersions are typically maintained at concentrations lower than 0.5 % w/v [10]. In our investigation, 1% w/v TOCNF suspension at 1.5 $mmol_{COOH}/g_{TOCNF}$ easily provided multi-particulate powder, with a high productivity. The hydrophilic nature of cellulosic materials implies a high capacity to retain water, leading to the necessity of operating at high process temperatures and low feed rates. This is why we set the temperature at 210–220 °C and the feed rate always lower than 5 mL/min (2–4 mL/min) obtaining the highest production yield when operating at 4 mL/min. The measured outlet temperature was in the range 110–120 °C, sufficient for efficient nanocellulose drying. The high temperatures required discouraged the use of this process for the drug encapsulation during the synthesis (the so-called pre-loading method) in the case of thermolabile drugs. The optimized process parameters after the first set of dry tests on TOCNF dispersions are shown in Table 2.

Table 2
Spray Drying process parameters.

Parameter	Fixed value
Inlet Temperature	210 °C
Feed rate	4 mL/min
TOCNF dispersions concentration	1 % w/V
TOCNF oxidation degree	1.5 $mmol_{COOH}/g_{TOCNF}$

The spray-dried TOCNF MS did not show any irreversible aggregation of particles commonly referred to as hornification [47,48]. In our case, MS showed no aggregation easy rewetting in aqueous solutions. A facile rewetting in water was also achieved after further freeze-drying, giving again the powder product for storage and subsequent analyses. Remarkably, no salt addition [9] was needed in our case to get the redispersion of dried MS in water.

Once optimized the process conditions (Table 2), we extended the MS production by SDT to those formulations containing bPEI as crosslinker and two different amounts of CA (see Table 1, entries 3 and 4). CA was added to increase the carboxylic functional groups content in the solution (see samples summary in Table 1). According to the eco-design of the nanostructured materials previously reported by our research group [49], the mass ratio between TOCNF and bPEI was maintained 1:1 for each suspension.

3.2. Microsponges morphological characterization

The morphological characterization was conducted by SEM, TEM and ADF STEM analysis. SEM allowed us to observe the 3D structure of particles, while TEM and ADF STEM microscopy highlighted both the nanostructure and the fibrous nature of the inner network of the MS. The SDT process parameters are known to influence the morphology of CNC- and CNF-based particles [50,51]. We used an experimental setup with a low feed rate (4 mL min^{-1}) and a high gas flow (530 L h^{-1}). Under these conditions, we processed 1% W/V TOCNF aqueous formulations, providing fibrous particles with a medium diameter of 2 μm. Fig. 1 A-B shows STEM images of the obtained TOCNF MS. The high inlet temperature and the selected low feed rate, which favoured the rapid and constant shrinking of droplets up to the complete solvent evaporation, provided a homogeneous population of particles. Generally, CNF treated by SDT tend to aggregate in almost spherical particles. Peng et al. reported that different process parameters led to particles with different morphologies from needle-like structures to irregular agglomerates, with medium lengths in the range of 4–20 μm and widths of 2–4 μm [18,

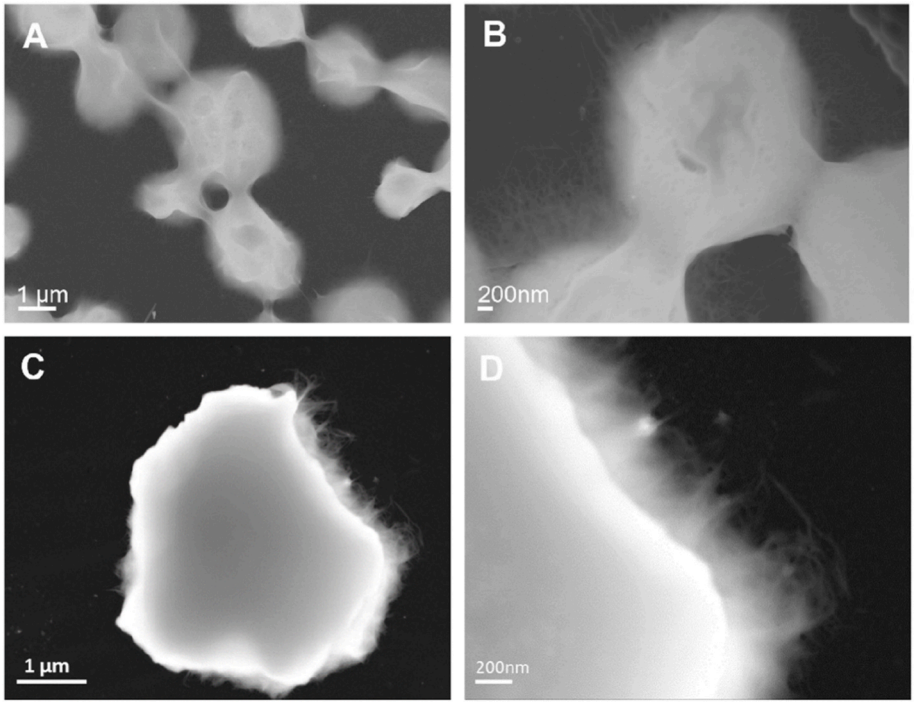

Fig. 1. ADF STEM images at different magnification of MS deriving from spray-dried TOCNF (A–B), and MS deriving from spray-dried bPEI modified-TOCNF (C–D). Scale bars are reported in each image.

Table 3
Statistical mean values of CE diameter and aspect ratios of dried TOCNF MS.

Dried MS	CE diameters mean (μm)	Aspect ratios mean
TOCNF MS	2.3 ± 0.5	0.97 ± 0.1
bPEI-TOCNF MS	3.4 ± 2.1	1.1 ± 0.3
bPEI-TOCNF@CA70 MS	3.1 ± 1.7	1 ± 0.2
bPEI-TOCNF@CA140 MS	4 ± 1.5	1 ± 0.2

52]. The proposed mechanism for TOCNF MS production is the formation of droplets in which nanofibers do not stretch out and are contained, providing a spherical structure. This is due to the short and skinny nature of the original fibers (TOCNF), as observed by TEM microscopy (Figure SI2 A). The resulting CNF entanglement in the droplet prevented the deformation, such as the donut shape, reported in the literature as the consequence of the resistance to the gas flow [52]. Additionally, TEM images revealed a "ball of wool" aspect of MS (see Figure SI1 B-C), while SEM images showed the presence of wrinkled surfaces (Figure SI3). A similar morphology was reported in the literature for different drug-loaded CNF microparticles with a diameter of around 5 μm [18]. A different morphology was observed when the formulations were processed in the presence of bPEI and CA. We observed more irregular particle shapes than those obtained from TOCNF suspensions (Fig. 1C–D), although the fibrous surface was maintained.

A similar morphology was observed for MS obtained by processing the two bPEI-TOCNF formulations containing CA (Table 1, entries 3 and 4), bPEI-TOCNF@CA70, and bPEI-TOCNF@CA140, (see STEM images in Figure SI4). Also in these cases, SEM analysis showed a smooth surface without the ridges previously observed in the TOCNF samples, thus confirming the hypothesis of a compact shape (Figure SI5). It is known how additives and covalent cross-linkers can influence the agglomeration of CNF during the SDT process [53–56]. In addition, previous studies have shown that the mechanical stability of this class of materials is improved by the formation of amide bonds between the COOH groups of the nanocellulose and the bPEI [31,32]. A similarly strong interaction could be expected to occur with the application of SDT. We

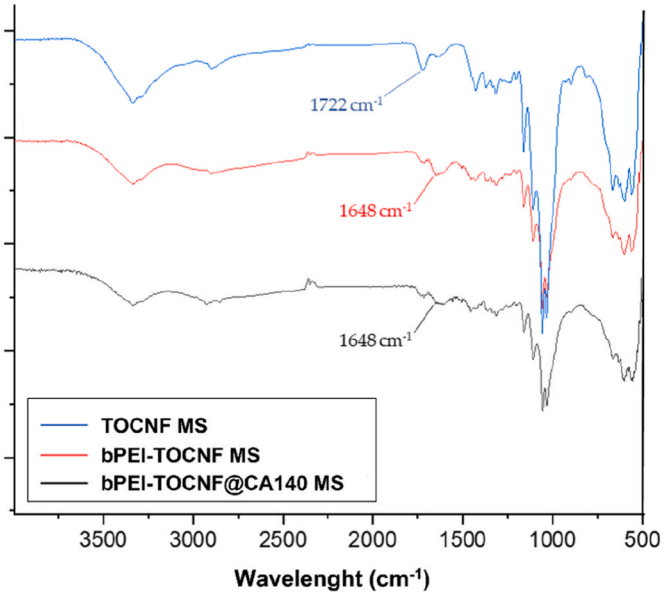

Fig. 2. FTIR spectrum of TOCNF MS (blue line), bPEI-TOCNF MS (red line), bPEI-TOCNF@CA140 MS (black line). (For interpretation of the references to color in this figure legend, the reader is referred to the Web version of this article.)

can speculate that the increased stiffness of the bPEI-modified TOCNF makes the chain folding process in the dry droplets more difficult during SDT, producing irregularly shaped and larger particles. The STEM analysis provided the statistical mean values of circle equivalent (CE) diameter and aspect ratios of dried MS. These values are reported in Table 3.

We observed the size increase by increasing the crosslinking degree of the spray-dried nanofibers in the presence of bPEI, moving from 2.3 ± 0.5 μm obtained for TOCNF MS to the 4.0 ± 1.5 μm for bPEI-

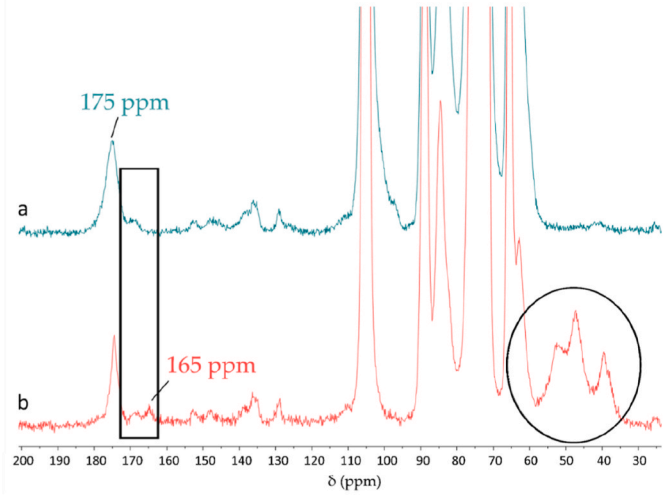

Fig. 3. ^{13}CP-MAS spectra of **a**) TOCNF MS and **b**) bPEI-TOCNF@CA140 MS.

Table 4
Crystallinity degrees of powders obtained with or without SDT.

Sample	Crystallinity Degree [%]	Obtained with STD
TOCNF MS	65.7	Y
bPEI-TOCNF@CA140 MS	66.4	Y
TOCNF	73.6	N

TOCNF@CA140 MS. This trend is consistent with the proposed mechanism of TOCNF folding inside the droplets during the drying step that is hampered by the stiffening effect of the crosslinking. Spectroscopic analysis was performed to verify the crosslinking by SDT of bPEI-TOCNF formulations.

3.3. Microsponges physical-chemical characterization

3.3.1. FT-IR, ^{13}C CP-MAS NMR spectroscopy and powder XRD analysis

FTIR and ^{13}C CP-MAS NMR were selected as techniques to verify the presence of amide bonds in the MS obtained by SDT. In Fig. 2 we report the spectra of TOCNF MS, bPEI-TOCNF MS and bPEI-TOCNF@CA140 MS. All samples were previously treated with HCl 0.1 N to achieve full protonation of COOH groups. TOCNF spectrum (Fig. 2, blue line) clearly shows the peak at 1722 cm^{-1} associated with the C═O stretching of the carboxylic acid moieties. In the spectra of Fig. 2, (bPEI-TOCNF MS and bPEI-TOCNF@CA140 MS, red line and black line respectively), the C═O signal related to the carboxyl groups (1722 cm^{-1}) is less pronounced and a signal can be detected at 1648 cm^{-1}. This latter frequency is related to the C═O stretching red shifted at lower wavelengths in the presence of the amidic group.

The ^{13}C CP-MAS NMR spectra are reported in Fig. 3. The assignments of the peaks associated with the carbons of the anhydroglucose units were supported by literature data [57]. The spectrum of Fig. 3a, related to the TOCNF MS, shows the typical peak of the carboxylate carbonyl carbon at 175 ppm. The spectrum reported in Fig. 3b of the sample bPEI-TOCNF@CA140 MS shows the weak but significant peak at 165 ppm, previously assigned to the amidic carbon [32], thus demonstrating covalent cross-linking of TOCNF by formation of amide bonds during the SDT process among the primary ammines of bPEI and the carboxylic groups of TOCNF and CA. Finally, the signals in the spectral region between 35 and 60 ppm can be assigned to the CH_2 carbons of the bPEI.

XRD analysis was also performed on samples TOCNF MS, bPEI-TOCNF@CA140 MS and TOCNF, to observe any variation in the TOCNF crystallinity before and after SDT. The degree of crystallinity was assessed with the method proposed by Park et al. (see SI for details) [58]. Accordingly, the powders produced with SDT showed a lower degree of crystallinity than pristine TOCNF (Table 4). Indeed, the increase of the amorphous contribution should be considered a pro for new carriers in terms of drug release efficiency [59,60].

Table 5
ζ-Potential of dilute TOCNF MS dispersions from DLS analysis[a].

SDT Microsponges	ζ-potential
TOCNF MS	−37.5 ± 0.5
bPEI-TOCNF MS	27.6 ± 1.5
bPEI-TOCNF@CA70 MS	19.2 ± 1.4
bPEI-TOCNF@CA140 MS	24.3 ± 0.9

[a] Mean values of 5 measurements consisting of 10 runs each.

3.3.2. Dynamic light scattering analysis

TOCNF MS obtained by the optimized SDT process can be easily dispersed in water without shape change or agglomeration. These features can be achieved with or without crosslinking agents in the formulation. It is important, at this stage, a thorough characterization of the stability and surface charge of the particles in water suspension. MS dispersions stability was evaluated via DLS analysis by measuring the surface charge [61]. The anionic nature of TOCNF was confirmed by measuring a ζ-potential value of −60 ± 1.8 mV on a diluted fibers water dispersion. Table 5 sums up the ζ-potential mean values of all the TOCNF MS dispersions.

The bPEI-TOCNF MS showed a positive charge due to a minor exposition of COOH groups following amide bond formation. These assessments could be useful for both the optimization of drug loading and to design chemical functionalization strategies [62]. The role of bPEI and CA in our SDT was widely investigated in the following physical-chemical and biological characterizations.

3.3.3. Swelling feature

The swelling ratios of produced MS were analysed by gravimetric method after their immersion in buffer solutions for 48 h. As can be observed in the plot of Fig. 4, TOCNF MS exhibited a slight pH-dependent behaviour. On the contrary, the swelling degree of bPEI-TOCNF-based MS significantly increased on going from pH 2 to 11, reaching the maximum at pH 7.5. In the presence of CA, sample swelling gradually increased reaching values over 800% at pH 11. This swelling feature as a function of the crosslinking density and pH has been discussed also for other polysaccharides-based particles and aerogels/cryogels [8,63,64]. The observed pH-sensitivity of bPEI-TOCNF-based MS was likely due to the content of both protonable ammine groups and deprotonated carboxylic groups [31]. The basic pH induces the formation of carboxylate anions from residual COOH groups not converted in the crosslinking reaction, allowing once again polysaccharide chains repulsions and relaxation [65]. This mechanism was also found for TOCNF-based hydrogel with 40% of deacetylated α-chitin nanofibers, which are rich in amine groups and hydroxyl groups [66]. The pH-sensitive swelling behaviour is an attractive feature for the controlled release of drugs into specific environments and/or cellular compartments. Our data indicate that the swelling ratios of crosslinked MS are higher than those of non-crosslinked MS, demonstrating the critical role of crosslinking in the design of a polymer scaffold for targeted applications [67].

The weak network structure resulting from the use of TOCNF could reduce the water holding capacity of the derived materials. This point was confirmed by the swelling studies performed in simulated gastric fluid (SGF) for 48 h at room temperature. The swelling ratios in SGF are reported in Table 6. The swelling degree in the presence of bPEI and CA was almost twice than that measured in TOCNF MS. This condition was investigated to work out the potential exploitation of TOCNF and their potential chemical modifications for gastric drug delivery.

The lowest swelling degree in SGF was detected for TOCNF MS. The

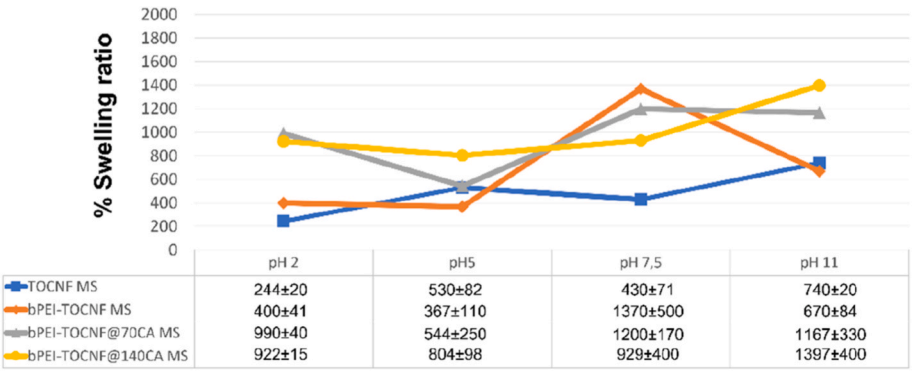

	pH 2	pH5	pH 7,5	pH 11
TOCNF MS	244±20	530±82	430±71	740±20
bPEI-TOCNF MS	400±41	367±110	1370±500	670±84
bPEI-TOCNF@70CA MS	990±40	544±250	1200±170	1167±330
bPEI-TOCNF@140CA MS	922±15	804±98	929±400	1397±400

Fig. 4. MS swelling behaviour after 48h in buffer solutions at the pH range 2–11.

Table 6
Swelling degree percentages of MS in simulated gastric fluid.

Sample	Swelling degree % in SGF
TOCNF MS	248 ± 4
bPEI-TOCNF MS	462 ± 60
bPEI-TOCNF@CA70 MS	500 ± 95
bPEI-TOCNF@CA140 MS	460 ± 140

protonation of TOCNF carboxyl groups in an acidic environment leads to a reduction in electrostatic repulsion. These weak electrostatic interactions would contribute to the development of hydrogen bonds between the protonated and deprotonated carboxyl groups, thus reducing the rate of penetration of SGF into the hydrogel matrix. This chemistry has been exploited for specific applications such as the delivery of probiotics [68,69]. The proposed mechanisms for swelling may be linked to drug loading and release processes, which have been studied exploiting the amphoteric nature of TC.

3.4. Drug loading study

In our procedure, TC loading occurs in aqueous MS suspension (overnight at RT) starting from an ethanol TC mother solution and reaching a final drug concentration of 0.5 mg/mL. This concentration is twice its water solubility (see paragraph 2.4). This factor could improve drug diffusion by capillary force across nanofibers matrix. The use of bPEI-based formulations allowed us to significantly improve TC adsorption: indeed, the loading efficiency was zero for TOCNF MS, but jumped to 70% for bPEI-TOCNF and bPEI-TOCNF@CA MS. Furthermore, analysis of the supernatant water after centrifugation showed no detectable amount of drug, suggesting that no significant release occurred during centrifugation. This efficient drug entrapment is probably due to swelling behaviour of the crosslinked MS and the favourable electrostatic interactions between TC and nanofibers. bPEI-TOCNF had a positive charge that can improve interaction with hydrophobic drugs [70]. In addition, TC is a pH dependent amphoteric molecule, it is present as cations at pH < 3.3, as zwitterions at pH between 3.3 and 7.7, and as anions at pH > 7.7 [36]. Loading procedure was performed in aqueous MS suspension. TOCNF MS aqueous suspension showed a negative ζ-potential and a pH $= 6$. The crosslinked MS exhibited a positive ζ-potential achieving a pH $= 8$. This pH variation tuned TC loading efficiency affecting electrostatic interactions between the molecule and MS matrixes. The role of the electrostatic interactions is confirmed by the null loading capability observed for the negatively charged TOCNF MS; in this case TC is exposed at neutral pH so it is present as zwitterion, with no net electrical charges. On the contrary, crosslinked MS have generated a favourable environment for the anionic form of the drug promoting its loading into positive charged carriers. Furthermore, water washing did not cause a detectable release of drug,

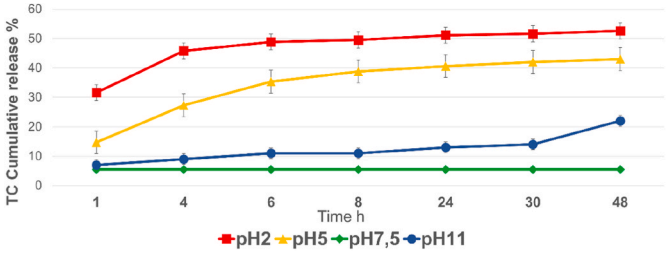

Fig. 5. Release profiles of TC from bPEI-TOCNF-based MS at different pH over time.

thus suggesting the persistence of physical interactions, both electrostatic and hydrophilic ones, in aqueous environment.

The loaded quantity determined by subtraction, was used to calculate loading capacity according to equation (3). As a result, bPEI-TOCNF and bPEI-TOCNF@CA MS had a loading capacity percentage of 7 %. A qualitative estimate of the drug loading was also achieved by thermogravimetric analysis on samples powder by comparing the thermal profiles of unloaded and TC-loaded MS. The TGA traces of all the MS samples with and without TC are reported in Figure SI 6. All the samples showed initial weight loss due to the removal of residual water from the synthesis and loading procedure. The comparison of the TGA traces obtained for TOCNF MS and TC-loaded analogue shows two quite similar, consistent with the limited loading capacity of the TOCNF MS previously assessed via spectrophotometric analysis. On the other hand, sensibly different weight-loss profiles are evident by comparing the TGA trace of bPEI-TOCNF MS with that of its TC-loaded analogue in the 100–200 °C temperature interval. This finding can be correlated to the TC loading. An analogous observation can be made comparing the TGA traces of MS with different amounts of CA (bPEI-TOCNF@CA140 MS and bPEI-TOCNF@CA70 MS) and their TC-loaded analogue showing features that might be ascribed to drug cargo. Moreover, the TGA traces of TOCNF MS shows a 5% weight loss at 100 °C attributable to dehydration, while the water loss observed for bPEI-TOCNF MS, bPEI-TOCNF@CA140 MS and bPEI-TOCNF@CA70 MS is in the range 15%–18%. This behaviour is due to the known hygroscopicity of the bPEI crosslinker and it is a hampering factor of the TC loading assessment by TGA.

3.5. Drug release in vitro study

In release study, 5 mg of TC-loaded samples were incubated in 1 ml of release medium for selected time intervals. Then, the supernatants containing the released drug were separated by centrifugation. Cumulative percentage release was calculated using equation (4). The 7% loading capacity value obtained by spectrophotometric measures (equation (3)) was used to calculate the TC amount per mg of MS to

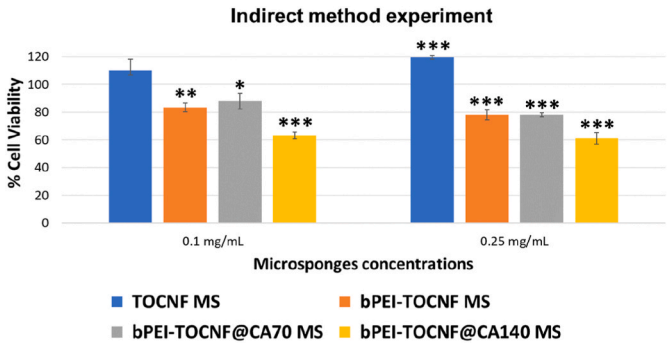

Fig. 6. Cells viability *versus* MS concentrations of conditioned medium after 24 h of treatment. Indirect method experiment has been performed incubating medium with TOCNF MS, bPEI-TOCNF MS, bPEI-TOCNF @CA70 MS and bPEI-TOCNF@CA140 MS suspensions at 0.1 and 0.25 mg/mL for 24h. Statistically significant value $p \leq 0.05$ (*), $p < 0.01$ (**) and $p < 0.001$ (***), with respect to not-treated condition, from T-test.

perform the release kinetic study. Accordingly, 7% of each sample was considered as the total amount of TC for all release experiments at variable pH conditions. The pH values were selected considering some *in vivo* conditions, such as topical and gastric applications, which suggest pH values in the range of 2–5. Neutral pH is the physiological condition and pH 11 was also considered as a comparison to interpret the physical-chemical behavior of produced particles. pH influenced remarkably the TC release, as indicated by the plots in Fig. 5 bPEI TOCNF MS presented a very low release capability (% cumulative release around 5) at pH 7.5 over 48h, in agreement to the high retention capability at this pH. On the contrary, a sustained release already in the first 4 h was found at acid pH, especially at pH 2. We verified a cumulative TC release after 1h of 32% and 15% at pH 2 and 5, respectively. The amount of released TC slowly raised to over 40% at these acid conditions. The promotion of drug release under acidic pH conditions could be caused by the dissociation of the electrostatic bonds between the positively charged bPEI TOCNF MS and TC in its zwitterionic form. The slow release rate from 4 h onwards was probably due to the nanostructured network preventing the burst release of poorly soluble drugs like TC, especially at high pH [71]. pH values above 7.7 forward the anionic form of TC intensifying the interactions with the positively charged MS which showed a very slow and low release.

A paradigmatic example of the interplay between the protonation state of TC and the sorption properties on a biochar surface is reported by Wang et al. [72]. A rapid kinetic was also found in SGF for all crosslinked MS, as reported in the following Table 7. TC molecules are all in cationic form at this condition, leading to the breakdown of electrostatic forces.

Release profiles of bPEI-TOCNF@CA-based MS did not differ much from bPEI-TOCNF-based ones as is shown by plots in Figure SI 7. The amount of CA had no effect on the TC loading efficiency nor the TC release profile, contrary to what observed for aerogels [31]. The *in vitro* release data suggested a pH responsive feature of synthetized TC-loaded MS that could be strategic for targeted drug delivery, considering that the observed responsivity at pH 1–5 could be useful for gastric and topical applications [51].

3.6. Biocompatibility study

In our investigation, the degree of oxidation of TOCNF showed a critical role in the SDT synthesis of MS. Recently, the importance of regeneration and degree of oxidation of cellulose MP for biomedical use has been demonstrated [73]. Here, we investigated the direct and indirect effect of TOCNF MS on human gastric cancer cells to understand the potential influence of crosslinking degree on cytocompatibility. The indirect contact method was carried out to evaluate the possible toxicity of the conditioned culture medium. Culture media were incubated for 24 h with all MS at 0.1 and 0.25 mg/mL. Centrifuged media were used to treat Kato III cells for 24 h. Cell viability percentage *versus* MS concentrations of the conditioned medium is reported in Fig. 6.

The histogram of Fig. 6 highlights the different behavior of TOCNF MS on the one side and the bPEI-derivatives on the other. TOCNF MS-conditioned medium had no cytotoxic effect, as shown by the blue bars of the histogram. Low cell viability decrease was observed for the other samples (see orange, gray and yellow). In particular, cell viability of 60% were measured for bPEI-TOCNF@CA140 MS conditioned sample, at both tested concentrations. All samples were washed after synthesis (as described in paragraph 2.2), and Cu^{2+}-complexation test excluded the presence of free b-PEI, so chemicals release could be ruled out. Conditioned culture media were assayed to measure pH and any significative pH change was detected for all samples. The indirect contact data suggested low cytotoxic effects of crosslinked MS, especially bPEI-TOCNF@CA140 MS, deriving from a potential deleterious interaction with culture medium (for example nutrient sequestration). Therefore, the direct contact experiment was performed with 0.01 mg/mL and 0.025 mg/mL of the four MS suspensions for 12 and 24h of treatment. The MTT results of Kato III cells are reported in Fig. 7. Cell viability remains up to 50% for all microparticles and conditions. TOCNF MS had no toxic effect on Kato III after 12 h of treatment for both tested concentrations. A low decrease of viability after 24 h of treatment was observed for all samples. bPEITOCNF@CA140 MS confirmed their moderate toxic effect (60% of cells viability) at both tested concentrations until after 12h of direct treatment. Also, bPEI-TOCNF@CA70 MS showed 60% of cells viability at the highest tested concentration, after

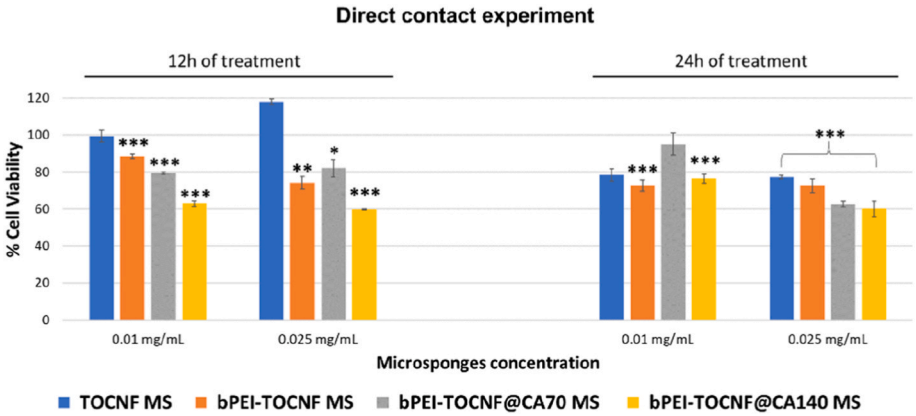

Fig. 7. Cells viability *versus* MS concentration after 12 and 24 h of treatment by direct contact with TOCNF MS, bPEI-TOCNF MS, bPEI-TOCNF@CA70 MS and bPEI-TOCNF@CA140 MS. Statistically significant value $p \leq 0.05$ (*), $p < 0.01$ (**) and $p < 0.001$ (***), respect to respective not-treated condition, from T-test.

Table 7
Tetracycline cumulative release percentages after 1h and 48h of incubation in simulated gastric fluid.

Samples	TC cumulative release after 1h in SGF	TC cumulative release after 48h in SGF
bPEI-TOCNF MS	44 %	52 %
bPEI-TOCNF@CA70 MS	50 %	60 %
bPEI-TOCNF@CA140 MS	50 %	60 %

24h.

These data suggest that the use of bPEI in the reticulation step did not significantly affect Kato III cell viability. Conversely, the CA co-presence in the crosslinking process should be carefully calibrated to avoid toxic effects, considering the viability decrease following both direct and indirect contact with bPEI- TOCNF@CA140 MS. This behavior could be explained by considering the physical-chemical features of the MS. TOCNF MS preserved the overall negative charge of the pristine nanofibers. This factor is an obstacle to the interaction with the negative cellular membrane. Conversely, the positive surface charge deriving from bPEI-based formulations could cause an electrostatic interaction with plasma membrane perturbing the physical-chemical equilibrium of cells. Furthermore, bPEI and CA modified MS showed the highest swelling degree at neutral and basic pH values, as previously discussed. The great swelling capacity of these MS could induce physical perturbation to cultured cells exerting a deleterious pressure, deriving from the enormous dimensions reached in the medium [74].

4. Conclusion

We have successfully prepared stable MS by spray drying suitable suspensions of TOCNF from cotton linters cellulose. This is the first report about Spray Drying manipulation of aqueous TOCNF dispersions with different oxidation degrees and crosslinkers quantities, using bPEI and CA. Nanofibers chemistry played a crucial role in SDT microparticles production. TOCNF dispersions with a carboxyl groups concentration of 1.5 $mmol_{COOH}/g_{TOCNF}$, provided the SDT formation of water-dispersible MS having an average diameter ranging from 2 to 4 μm and a "ball of wool" aspect. MS from TOCNF dispersions were more spherical and monodisperse, and smaller than those deriving from bPEI and CA-based formulations. The crosslinking during SDT process was confirmed by spectroscopic analysis detecting the formation of amide bonds. The loading and release patterns of TC are strictly dependent on the electrostatic interactions between the molecule and the MS nanofibers. Furthermore, a pH-responsive swelling and release behaviour was found for crosslinked MS. Finally, cell viability data revealed moderate cytotoxicity following contact with TOCNF MS containing CA, probably due to a synergistic effect of mechanical perturbation and interaction with the culture medium in the verified swollen state. Our results showed that crosslinkers are not required to effectively dry TOCNF by producing stable suspensions of MS in water, in contrast to what has been observed for aerogels. However, the presence of b-PEI and CA can modulate the morphology, degree of swelling, drug entrapment and cytocompatibility of spray-dried MS. From this perspective, chemical crosslinking is a critical step in the design and synthetic strategies of novel TOCNF-based systems for controlled drug delivery.

Author contributions

Andrea Fiorati: Conceptualization, Investigation, Writing - Original Draft, Writing - Review & Editing. Francesca Baldassarre: Conceptualization, Methodology, Validation, Investigation, Data Curation, Writing - Original Draft, Writing - Review & Editing, Visualization. Laura Riva: Investigation, Validation, Writing - Review & Editing. Stefano Tacconi: Investigation, Validation, Formal analysis. Concetta Nobile: Investigation. Viviana Vergaro: Investigation, Writing - Review & Editing. Roberto Grisorio: Investigation, Data Curation. Lucio Melone: Writing - Review & Editing, Supervision, Funding acquisition. Andrea Mele: Writing - Review & Editing, Supervision, Funding acquisition. Luciana Dini: Data Curation, Supervision. Carlo Punta: Data Curation, Writing - Review & Editing, Supervision, Funding acquisition. Giuseppe Ciccarella: Writing - Review & Editing, Supervision, Funding acquisition, Project administration.

Declaration of competing interest

The authors declare that they have no known competing financial interests or personal relationships that could have appeared to influence the work reported in this paper.

Data availability

All data have been reported in the manuscript and in supporting material.

Acknowledgments

We thank Prof. Gian Paolo Suranna for useful discussions and critical reading of the manuscript.

This work was supported by Regione Puglia, Project Research for innovation (REFIN) "SINTESI DI UN SISTEMA TERANOSTICO A BASE DI NANO-CELLULOSA PER LA DETECTION E LA CURA DEI TUMORI" (code: 0B988883); MINISTERO DELL'ISTRUZIONE, DELL'UNIVERSITA' E DELLA RICERCA, Project NanotEcnologie chiMiche green per la protEzione Sostenibile delle pIante (NEMESI) ARS01_01002 CUP: F36C18000180005, Piano Nazionale della Ricerca, PNR—Chimica verde; Regione Lombardia, RL-INSTM Call2016, Project "NAno-cellulosa da fonti rInnovabili per la somministrAzione sostenibile Di fitofarmacI"-NAIADI.

LIST OF ABBREVIATIONS

bPEI	branched polyethylenimine.
CA	citric acid
CNC	cellulose nanocrystals
CNF	cellulose nanofibers
TEMPO	(2,2,6,6-tetramethylpiperidine-1-oxyl)-mediated oxidation
TOCNF	TEMPO-oxidized cellulose nanofibers
bPEI-TOCNF	bPEI-modified TEMPO-oxidized cellulose nanofibers
bPEI-TOCNF@CA70	bPEI-modified TEMPO-oxidized cellulose nanofibers with 70 mg CA
bPEI-TOCNF@CA140	bPEI-modified TEMPO-oxidized cellulose nanofibers with 140 mg CA
MS	microsponges
bPEI-TOCNF	MS microsponges derived from bPEI-TOCNF Spray Drying
bPEI-TOCNF@CA70 MS	microsponges derived from bPEI-TOCNF@CA70 Spray Drying
bPEI-TOCNF@CA140 MS	microsponges derived from bPEI-TOCNF@CA140 Spray Drying
SGF	simulated gastric fluid
SDT	Spray Drying Technology
TC	tetracycline.

Appendix A. Supplementary data

Supplementary data to this article can be found online at https://doi.org/10.1016/j.jddst.2023.105080.

References

[1] R.A.M. Osmani, et al., Microsponge based drug delivery system for augmented gastroparesis therapy: formulation development and evaluation, Asian J. Pharm. Sci. 10 (5) (2015) 442–451, https://doi.org/10.1016/j.ajps.2015.06.003.

[2] M. Akram, et al., Sustained release of hydrophilic drug from polyphosphazenes/poly(methyl methacrylate) based microspheres and their degradation study, Mater. Sci. Eng. C 58 (2016) 169–179, https://doi.org/10.1016/j.msec.2015.08.010.

[3] C. Gómez-Gaete, M. Retamal, C. Chávez, P. Bustos, R. Godoy, P. Torres-Vergara, Development, characterization and in vitro evaluation of biodegradable rhein-loaded microparticles for treatment of osteoarthritis, Eur. J. Pharmaceut. Sci. 96 (2017) 390–397, https://doi.org/10.1016/j.ejps.2016.10.010.

[4] M. Nidhi, V. Rashid, S. Kaur, S. Hallan, S. Sharma, N. Mishra, Microparticles as controlled drug delivery carrier for the treatment of ulcerative colitis: a brief review, Saudi Pharmaceut. J. 24 (4) (Jul. 2016) 458–472, https://doi.org/10.1016/j.jsps.2014.10.001.

[5] L. Druel, A. Kenkel, V. Baudron, S. Buwalda, T. Budtova, Cellulose aerogel microparticles via emulsion-coagulation technique, Biomacromolecules 21 (5) (May 2020) 1824–1831, https://doi.org/10.1021/acs.biomac.9b01725.

[6] W.-H. Lin, S.C. Jana, Analysis of porous structures of cellulose aerogel monoliths and microparticles, Microporous Mesoporous Mater. 310 (2021), 110625, https://doi.org/10.1016/j.micromeso.2020.110625.

[7] Y. Chen, et al., Recent progress on nanocellulose aerogels: preparation, modification, composite fabrication, applications, Adv. Mater. 33 (11) (Mar. 2021), 2005569, https://doi.org/10.1002/adma.202005569.

[8] H. Cai, et al., Aerogel microspheres from natural cellulose nanofibrils and their application as cell culture scaffold, Biomacromolecules 15 (7) (Jul. 2014) 2540–2547, https://doi.org/10.1021/bm5003976.

[9] G. Kaufman, et al., Highly stiff yet elastic microcapsules incorporating cellulose nanofibrils, Soft Matter 13 (15) (2017) 2733–2737, https://doi.org/10.1039/C7SM00092H.

[10] T. Paulraj, A. v Riazanova, K. Yao, R.L. Andersson, A. Müllertz, A.J. Svagan, Bioinspired layer-by-layer microcapsules based on cellulose nanofibers with switchable permeability, Biomacromolecules 18 (4) (Apr. 2017) 1401–1410, https://doi.org/10.1021/acs.biomac.7b00126.

[11] K. Löbmann, A.J. Svagan, Cellulose nanofibers as excipient for the delivery of poorly soluble drugs, Int. J. Pharm. 533 (1) (2017) 285–297, https://doi.org/10.1016/j.ijpharm.2017.09.064.

[12] S. Fujisawa, E. Togawa, K. Kuroda, T. Saito, A. Isogai, Fabrication of ultrathin nanocellulose shells on tough microparticles via an emulsion-templated colloidal assembly: towards versatile carrier materials, Nanoscale 11 (Aug) (2019), https://doi.org/10.1039/C9NR02612F.

[13] G. Pierre, et al., TEMPO-mediated oxidation of polysaccharides: an ongoing story, Carbohydr. Polym. 165 (2017) 71–85, https://doi.org/10.1016/j.carbpol.2017.02.028.

[14] S. Fujisawa, T. Isogai, and A. Isogai, 'Temperature and pH Stability of Cellouronic Acid', doi: 10.1007/s10570-010-9407-9.

[15] Y. Kobayashi, T. Saito, A. Isogai, Aerogels with 3D ordered nanofiber skeletons of liquid-crystalline nanocellulose derivatives as tough and transparent insulators, Angew. Chem. Int. Ed. 53 (39) (Sep. 2014) 10394–10397, https://doi.org/10.1002/anie.201405123.

[16] F. Jiang, Y.-L. Hsieh, Super water absorbing and shape memory nanocellulose aerogels from TEMPO-oxidized cellulose nanofibrils via cyclic freezing–thawing, J Mater Chem A Mater 2 (2) (2014) 350–359, https://doi.org/10.1039/C3TA13629A.

[17] C.A. García-González, M. Alnaief, I. Smirnova, Polysaccharide-based aerogels - promising biodegradable carriers for drug delivery systems- Review Article, Carbohydr. Polym. 86 (Oct. 2011) 1425–1438, https://doi.org/10.1016/j.carbpol.2011.06.066.

[18] R. Kolakovic, T. Laaksonen, L. Peltonen, A. Laukkanen, J. Hirvonen, Spray-dried nanofibrillar cellulose microparticles for sustained drug release, Int. J. Pharm. 430 (1) (2012) 47–55, https://doi.org/10.1016/j.ijpharm.2012.03.031.

[19] L.L. Messa, R. Faez, Spray-dried chitosan/nanocellulose microparticles: synergistic effects for the sustained release of NPK fertilizer, Cellulose 27 (17) (2020) 10077–10093, https://doi.org/10.1007/s10570-020-03482-2.

[20] D. França, J.R.S. de Barros, R. Faez, Spray-dried cellulose nanofibrils microparticles as a vehicle for enhanced efficiency fertilizers, Cellulose 28 (3) (2021) 1571–1585, https://doi.org/10.1007/s10570-020-03609-5.

[21] A.B. Meneguin, et al., Spray-dried bacterial cellulose nanofibers: a new generation of pharmaceutical excipient intended for intestinal drug delivery, Carbohydr. Polym. 249 (2020), 116838, https://doi.org/10.1016/j.carbpol.2020.116838.

[22] Z. Pakowski, Modern methods of drying nanomaterials, Transport Porous Media 66 (1) (2007) 19–27, https://doi.org/10.1007/s11242-006-9019-x.

[23] V. Vergaro, et al., Scalable production of calcite nanocrystals by atomization process: synthesis, characterization and biological interactions study, Adv. Powder Technol. 28 (10) (2017), https://doi.org/10.1016/j.apt.2016.12.018.

[24] F. Baldassarre, et al., Biocatalytic synthesis of phospholipids and their application as coating agents for CaCO3 nano–crystals: characterization and intracellular localization analysis, ChemistrySelect 1 (20) (2016), https://doi.org/10.1002/slct.201601429.

[25] K. Samborska, et al., Innovations in spray drying process for food and pharma industries, J. Food Eng. 321 (2022), 110960, https://doi.org/10.1016/j.jfoodeng.2022.110960.

[26] M.C.I.M. Amin, A.G. Abadi, H. Katas, Purification, characterization and comparative studies of spray-dried bacterial cellulose microparticles, Carbohydr. Polym. 99 (2014) 180–189, https://doi.org/10.1016/j.carbpol.2013.08.041.

[27] Y. Peng, Y. Han, D. Gardner, Spray-drying cellulose nanofibrils: effect of drying process parameters on particle morphology and size distribution, Wood Fiber Sci. 44 (Oct. 2012) 448–461.

[28] B. Liu and Y. Huang, 'Polyethyleneimine Modified Eggshell Membrane as a Novel Biosorbent for Adsorption and Detoxification of Cr(VI) from Water †', doi: 10.1039/c1jm12329g.

[29] Y. Xie, C.A.S. Hill, Z. Xiao, H. Militz, C. Mai, Silane coupling agents used for natural fiber/polymer composites: a review, Compos Part A Appl Sci Manuf 41 (7) (2010) 806–819, https://doi.org/10.1016/j.compositesa.2010.03.005.

[30] W. Zhou, Effect of coupling agents on the thermal conductivity of aluminum particle/epoxy resin composites, J. Mater. Sci. 46 (Jun. 2011) 3883–3889, https://doi.org/10.1007/s10853-011-5309-y.

[31] A. Fiorati, et al., Mechanical and drug release properties of sponges from cross-linked cellulose nanofibers, Chempluschem 82 (6) (Jun. 2017) 848–858, https://doi.org/10.1002/cplu.201700185.

[32] L. Melone, B. Rossi, N. Pastori, W. Panzeri, A. Mele, C. Punta, TEMPO-oxidized cellulose cross-linked with branched polyethyleneimine: nanostructured adsorbent sponges for water remediation, Chempluschem 80 (9) (Sep. 2015) 1408–1415, https://doi.org/10.1002/cplu.201500145.

[33] L. Melone, S. Bonafede, D. Tushi, C. Punta, M. Cametti, Dip in colorimetric fluoride sensing by a chemically engineered polymeric cellulose/bPEI conjugate in the solid state, RSC Adv. 5 (101) (2015) 83197–83205, https://doi.org/10.1039/C5RA16764G.

[34] L. Riva, A. Fiorati, A. Sganappa, L. Melone, C. Punta, M. Cametti, Naked-eye heterogeneous sensing of fluoride ions by Co-polymeric nanosponge systems comprising aromatic-imide-functionalized nanocellulose and branched polyethyleneimine, Chempluschem 84 (10) (Oct. 2019) 1512–1518, https://doi.org/10.1002/cplu.201900348.

[35] L. Riva, C. Punta, A. Sacchetti, Co-polymeric nanosponges from cellulose biomass as heterogeneous catalysts for amine-catalyzed organic reactions, ChemCatChem 12 (24) (Dec. 2020) 6214–6222, https://doi.org/10.1002/cctc.202001157.

[36] Z. Li, L. Schulz, C. Ackley, N. Fenske, Adsorption of tetracycline on kaolinite with pH-dependent surface charges, J. Colloid Interface Sci. 351 (1) (2010) 254–260, https://doi.org/10.1016/j.jcis.2010.07.034.

[37] P.W. Wertz, R.E. Tao, S. Prajapati, J.N. Pixley, A. Grada, S.R. Feldman, Oral Tetracycline-Class Drugs in Dermatology: Impact of Food Intake on Absorption and Efficacy, 2023, https://doi.org/10.3390/antibiotics12071152.

[38] M.R. Acharya, J. Venitz, W.D. Figg, A. Sparreboom, Chemically modified tetracyclines as inhibitors of matrix metalloproteinases, Drug Resist. Updates 7 (3) (2004) 195–208, https://doi.org/10.1016/j.drup.2004.04.002.

[39] A. Isogai, T. Saito, H. Fukuzumi, TEMPO-oxidized cellulose nanofibers, Nanoscale 3 (Oct. 2010) 71–85, https://doi.org/10.1039/c0nr00583e.

[40] J. Xu, X. Tan, L. Chen, X. Li, F. Xie, Starch/microcrystalline cellulose hybrid gels as gastric-floating drug delivery systems, Carbohydr. Polym. 215 (2019) 151–159, https://doi.org/10.1016/j.carbpol.2019.03.078.

[41] R. Grisorio, et al., Influence of keto groups on the optical, electronic, and electroluminescent properties of random fluorenone-containing poly(fluorenylene-vinylene)s, J. Phys. Chem. C 112 (50) (Dec. 2008) 20076–20087, https://doi.org/10.1021/jp806879c.

[42] N.O. Okamoto-Schalch, S.G.B. Pinho, T.T. de Barros-Alexandrino, G.C. Dacanal, O. B.G. Assis, M. Martelli-Tosi, Production and characterization of chitosan-TPP/cellulose nanocrystal system for encapsulation: a case study using folic acid as active compound, Cellulose 27 (10) (2020) 5855–5869, https://doi.org/10.1007/s10570-020-03173-y.

[43] Y. Yuan, J. Huang, S. He, M. Ma, D. Wang, Y. Xu, One-step self-assembly of curcumin-loaded zein/sophorolipid nanoparticles: physicochemical stability, redispersibility, solubility and bioaccessibility, Food Funct. 12 (13) (2021) 5719–5730, https://doi.org/10.1039/D1FO00942G.

[44] Y. Yuan, S. Zhang, M. Ma, D. Wang, Y. Xu, Encapsulation and delivery of curcumin in cellulose nanocrystals nanoparticles using pH-driven method, LWT 155 (2022), 112863, https://doi.org/10.1016/j.lwt.2021.112863.

[45] P. Subhedar, J.B. Naik, D.N. Muley, Effect of polymer concentration on sustained release microparticles of metformin hydrochloride prepared by using spray dryer, Polym. Plast. Technol. Eng. 49 (3) (Jan. 2010) 267–271, https://doi.org/10.1080/03602550903413896.

[46] N. Grattard, M. Pernin, B. Marty, G. Roudaut, D. Champion, M. Le Meste, Study of release kinetics of small and high molecular weight substances dispersed into spray-dried ethylcellulose microspheres, J. Contr. Release 84 (3) (2002) 125–135, https://doi.org/10.1016/S0168-3659(02)00260-2.

[47] E.-L. Hult, P. Larsson, T. Iversen, Cellulose fibril aggregation - an inherent property of kraft pulps, Polymer (Guildf) 42 (Apr. 2001) 3309–3314, https://doi.org/10.1016/S0032-3861(00)00774-6.

[48] S. Iwamoto, K. Abe, H. Yano, The effect of hemicelluloses on wood pulp nanofibrillation and nanofiber network characteristics, Biomacromolecules 9 (3) (Mar. 2008) 1022–1026, https://doi.org/10.1021/bm701157n.

[49] A. Fiorati, et al., Eco-design of nanostructured cellulose sponges for sea-water decontamination from heavy metal ions, J. Clean. Prod. 246 (2020), 119009, https://doi.org/10.1016/j.jclepro.2019.119009.

[50] R. Nagula, S. Wairkar, Cellulose microsponges based gel of naringenin for atopic dermatitis: design, optimization, in vitro and in vivo investigation, Int. J. Biol. Macromol. 164 (Jul) (2020), https://doi.org/10.1016/j.ijbiomac.2020.07.168.

[51] M. Jafar, A. Mohsin, M. Khalid, A. Alshahrani, F. Alkhateeb, A. Alqarni, Ranitidine hydrochloride stomach specific buoyant microsponge: preparation, in-vitro characterization, and in-vivo anti-ulcer activity, J. Drug Deliv. Sci. Technol. 55 (Dec. 2019), 101453, https://doi.org/10.1016/j.jddst.2019.101453.

[52] Y. Peng, D.J. Gardner, Y. Han, Drying cellulose nanofibrils: in search of a suitable method, Cellulose 19 (1) (2012) 91–102, https://doi.org/10.1007/s10570-011-9630-z.
[53] G. Yang, et al., Comparison of effects of sodium chloride and potassium chloride on spray drying and redispersion of cellulose nanofibrils suspension, Nanomaterials 11 (2) (2021), https://doi.org/10.3390/nano11020439.
[54] Y. Peng, S.A. Gallegos, D.J. Gardner, Y. Han, Z. Cai, Maleic anhydride polypropylene modified cellulose nanofibril polypropylene nanocomposites with enhanced impact strength, Polym. Compos. 37 (3) (Mar. 2016) 782–793, https://doi.org/10.1002/pc.23235.
[55] S. Sungsinchai, C. Niamnuy, P. Wattanapan, M. Charoenchaitrakool, S. Devahastin, Spray drying of non-chemically prepared nanofibrillated cellulose: improving water redispersibility of the dried product, Int. J. Biol. Macromol. 207 (2022) 434–442, https://doi.org/10.1016/j.ijbiomac.2022.02.153.
[56] T.H. Kim, S.-H. Lee, J.-C. Kim, Spray-dried microparticles composed of carboxylated cellulose nanofiber and cysteamine and their oxidation-responsive release property, Colloid Polym. Sci. 298 (2) (2020) 157–167, https://doi.org/10.1007/s00396-019-04591-6.
[57] E. Vismara, L. Melone, G. Gastaldi, C. Cosentino, G. Torri, Surface functionalization of cotton cellulose with glycidyl methacrylate and its application for the adsorption of aromatic pollutants from wastewaters, J. Hazard Mater. (2009), https://doi.org/10.1016/j.jhazmat.2009.05.042.
[58] S. Park, J.O. Baker, M.E. Himmel, P.A. Parilla, D.K. Johnson, Cellulose crystallinity index: measurement techniques and their impact on interpreting cellulase performance, Biotechnol. Biofuels 3 (1) (2010) 10, https://doi.org/10.1186/1754-6834-3-10.
[59] V. Karavelidis, E. Karavas, D. Giliopoulos, S. Papadimitriou, D. Bikiaris, Evaluating the effects of crystallinity in new biocompatible polyester nanocarriers on drug release behavior, Int. J. Nanomed. 6 (2011) 3021–3032, https://doi.org/10.2147/IJN.S26016.
[60] F. Alexis, Factors affecting the degradation and drug-release mechanism of poly (lactic acid) and poly[(lactic acid)-co-(glycolic acid)], Polym. Int. 54 (1) (2005) 36–46, https://doi.org/10.1002/pi.1697.
[61] F. Baldassarre, M. Cacciola, G. Ciccarella, A predictive model of iron oxide nanoparticles flocculation tuning Z-potential in aqueous environment for biological application, J. Nanoparticle Res. 17 (9) (2015), https://doi.org/10.1007/s11051-015-3163-6.
[62] V. Vergaro, et al., CaCO3 as an environmentally friendly renewable material for drug delivery systems: uptake of HSA-CaCO3 nanocrystals conjugates in cancer cell lines, Materials 12 (9) (2019), https://doi.org/10.3390/ma12091481.
[63] J. Li, Y. Wang, L. Zhang, Z. Xu, H. Dai, W. Wu, Nanocellulose/gelatin composite cryogels for controlled drug release, ACS Sustain. Chem. Eng. 7 (6) (Mar. 2019) 6381–6389, https://doi.org/10.1021/acssuschemeng.9b00161.
[64] T. Anirudhan, B. Jayan, C. John, Multi-polysaccharide based stimuli responsive polymeric network for the: in vitro release of 5-fluorouracil and levamisole hydrochloride, New J. Chem. 41 (Sep) (2017), https://doi.org/10.1039/C7NJ01745F.
[65] I.M. El-Sherbiny, H.D.C. Smyth, Controlled release pulmonary administration of curcumin using swellable biocompatible microparticles, Mol. Pharm. 9 (2) (Feb. 2012) 269–280, https://doi.org/10.1021/mp200351y.
[66] J. Xu, et al., Engineering biocompatible hydrogels from bicomponent natural nanofibers for anticancer drug delivery, J. Agric. Food Chem. 66 (4) (Jan. 2018) 935–942, https://doi.org/10.1021/acs.jafc.7b04210.
[67] Y. Fu, W.J. Kao, Drug release kinetics and transport mechanisms of non-degradable and degradable polymeric delivery systems, Expet Opin. Drug Deliv. 7 (4) (Apr. 2010) 429–444, https://doi.org/10.1517/17425241003602259.
[68] M. Karzar Jeddi, M. Mahkam, Magnetic nano carboxymethyl cellulose-alginate/chitosan hydrogel beads as biodegradable devices for controlled drug delivery, Int. J. Biol. Macromol. 135 (2019) 829–838, https://doi.org/10.1016/j.ijbiomac.2019.05.210.
[69] H. Zhang, et al., A pH-responsive gel macrosphere based on sodium alginate and cellulose nanofiber for potential intestinal delivery of probiotics, ACS Sustain. Chem. Eng. 6 (11) (Nov. 2018) 13924–13931, https://doi.org/10.1021/acssuschemeng.8b02237.
[70] N. Zainuddin, I. Ahmad, H. Kargarzadeh, S. Ramli, Hydrophobic kenaf nanocrystalline cellulose for the binding of curcumin, Carbohydr. Polym. 163 (2017) 261–269, https://doi.org/10.1016/j.carbpol.2017.01.036.
[71] H. Paukkonen, et al., Nanofibrillar cellulose hydrogels and reconstructed hydrogels as matrices for controlled drug release, Int. J. Pharm. 532 (1) (2017) 269–280, https://doi.org/10.1016/j.ijpharm.2017.09.002.
[72] H. Wang, et al., Sorption of Tetracycline on Biochar Derived from Rice Straw and Swine Manure †, 2018, https://doi.org/10.1039/c8ra01454j.
[73] U. Aydemir Sezer, İ. Sahin, B. Aru, H. Olmez, G. Yanıkkaya Demirel, S. Sezer, Cytotoxicity, bactericidal and hemostatic evaluation of oxidized cellulose microparticles: structure and oxidation degree approach, Carbohydr. Polym. 219 (2019) 87–94, https://doi.org/10.1016/j.carbpol.2019.05.005.
[74] M. Pandey, N. Mohamad, W.-L. Low, C. Martin, M.C.I. Mohd Amin, Microwaved bacterial cellulose-based hydrogel microparticles for the healing of partial thickness burn wounds, Drug Deliv Transl Res 7 (1) (2017) 89–99, https://doi.org/10.1007/s13346-016-0341-8.